Electrochemical and Solid-State Letters, **14** (1) P1-P4 (2011)
1099-0062/2010/14(1)/P1/4/$28.00 © The Electrochemical Society

First-Principles Prediction of Optical Absorption Enhancement for Si Native Defect Clusters under Biaxial Strain

Robert J. Bondi, Sangheon Lee, and Gyeong S. Hwang[z]

Department of Chemical Engineering, University of Texas, Austin, Texas 78712, USA

We use density-functional theory calculations to qualitatively explore the effects of fourfold-coordinated vacancy (V_4) and interstitial (I_4) clusters on optical absorption spectra in crystalline Si (c-Si) under selected conditions of biaxial strain ($\varepsilon = -3$, 0, and 3%). While both native defect clusters enhance c-Si absorption by redshifting the absorption edge, we observe additional enhancement from biaxial strain. Increased strain magnitude tends to increase the absorption enhancement effect, but the optimal sign of strain exhibits a complementary relationship: compressive strain most effectively enhances V_4 absorption, while tensile strain most effectively enhances I_4 absorption. The absorption redshift as a function of strain correlates well with effective bandgap reduction, including the appearance of an intermediate band under certain conditions ($\varepsilon = -3$ and 0%) for V_4. Our results suggest that manipulation of native defect distributions and their strain fields can be used to engineer the Si absorption spectra.
 [DOI: 10.1149/1.3511714]

Manuscript submitted August 31, 2010; revised manuscript received October 14, 2010. Published November 10, 2010.

Improvement in the net efficiency of crystalline Si (c-Si) solar cells has been impeded by intrinsic properties including low absorption and a bandgap (E_g) precluding photogeneration of carriers in the infrared. Low optical absorption inflates solar module cost by requiring thick substrates (~ 100 μm)[1] and has consequently generated strong interest in derivative thin film materials, such as hydrogenated amorphous Si (a-Si:H),[2] which significantly reduce the requisite substrate thickness (~ 1 μm)[1,3] through a serendipitous redshift of the absorption coefficient that accompanies disintegration of long range order. Other techniques to improve c-Si absorption include transition metal doping to create intermediate bands (IBs) (Ref. 4 and 5) and growth of Si nanowire arrays that promote broadband absorption.[6]

Optical methods[1] provide a non-destructive means of semiconductor characterization because optical properties are derived from electronic structure. Variations in phase[3] and defect-content[7,8] of Si produce significant changes in the optical absorption spectra, which suggests the plausibility of defect engineering[9] the spectra through structural manipulation. While c-Si absorption[10] is negligible below the 1.11 eV experimental bandgap,[11] Si absorption at lower energies is attainable through the participation of band tail extended states (Urbach region) or at even lower energies in the presence of localized defects, such as native defect clusters, that can generate states near the Fermi level.[7] The recent theoretical work of Pan et al.[12] elucidates an atomistic topological relationship connecting short (long) Si-Si bonds with valence (conduction) band character in the electronic structure of amorphous Si (a-Si), which suggests that control of strain distributions can modify the joint density of states and resultant optical absorption.

In this article, we discuss the first-principles prediction of enhanced Si optical absorption in the presence of native defects in which local strain fields are further modified by applied biaxial strain. In particular, we present calculated optical spectra for the absorption coefficient, $\alpha(\omega)$, for previously-identified fourfold-coordinated (FC) defect clusters composed of four vacancies (V_4) and four interstitials (I_4) and show how applied biaxial strain further modifies optical absorption relative to c-Si. In addition, we use local density of states (LDOS) calculations to indicate the qualitative relationship between structural strain and the electronic structure governing optical transitions.

The atomic configurations, electronic structures, and optical spectra reported herein were calculated using a planewave pseudopotential method within the generalized gradient approximation of Perdew and Wang (GGA-PW91) (Ref. 13) to density-functional theory (DFT),[14] as implemented in the Vienna ab-initio simulation package.[15] The projector-augmented wave method[16] was used to describe the interaction between ion cores and valence electrons. Kinetic energy cut-offs of 250 and 300 eV were used on the plane-wave basis set during ionic relaxation and for electronic calculations, respectively. Brillouin zone sampling was accomplished during ionic relaxation using one k-point (Γ) until residual forces had converged within 5×10^{-2} eV/Å tolerance. The k-point sampling scheme was increased to a $3 \times 3 \times 3$ Monkhorst-Pack mesh for electronic and optical calculations on the optimized structures. Transition energies were sampled up to 20 eV using 750 conduction bands and the OPTICS code of Furthmüller[17] was employed to compute the real (ε_1) and imaginary (ε_2) parts of the frequency-dependent dielectric function, $\varepsilon(\omega)$. We performed preliminary calculations to ensure convergence of both the optical spectra and low-frequency dielectric constant (ε_o) as a function of conduction bands. The absorption coefficient was subsequently computed from $\varepsilon(\omega)$ as

$$\alpha(\omega) = \frac{\sqrt{2}E}{\hbar}\left[\sqrt{\varepsilon_1^2(\omega) + \varepsilon_2^2(\omega)} - \varepsilon_1(\omega)\right]^{1/2} \quad [1]$$

where E represents photon energy and $\hbar$ represents the reduced Planck's constant. We describe this optical calculation methodology based on the independent-particle approximation in more detail in our previous work.[18,19]

The density-functional theory-generalized gradient approximation (DFT-GGA) approach employed here characteristically underestimates E_g, but the resulting qualitative trends are considered reliable. Numerous correction methods exist to address the electronic structure deficiencies of DFT, but each method necessitates additional trade-offs. Hybrid functionals use a mixture of Hartree-Fock (HF) exchange-correlation with local or semilocal density functionals (GGA) to improve E_g representations, but HF evaluation in periodic systems can be computationally expensive and the ratio of HF/DFT representation is an additional variable.[20] The quasiparticle GW method (G represents Green function, W represents a screened Coulomb potential) demands significantly more computational expense because the solution of single-particle Kohn-Sham equations in DFT is supplanted by calculation of both the dielectric function and single-particle Green function via rigorous solution of the Dyson equation.[21] Application of either correction method here would be cost-prohibitive because of the large supercells required to represent defect clusters. Despite acknowledged deficiencies, DFT calculations using local or semilocal density functionals have been used extensively in qualitative descriptions of electrical, optical, and magnetic properties in diverse material systems.[22-26]

A DFT-optimized lattice constant (a_{Si}) of 5.457 Å along ⟨100⟩ was used to construct the strain-free Si supercell. Using linear elastic theory,[27,28] we implement uniform biaxial strain in 480-atom basis supercells through dimensional control by determining the re-

[z] E-mail: gshwang@che.utexas.edu

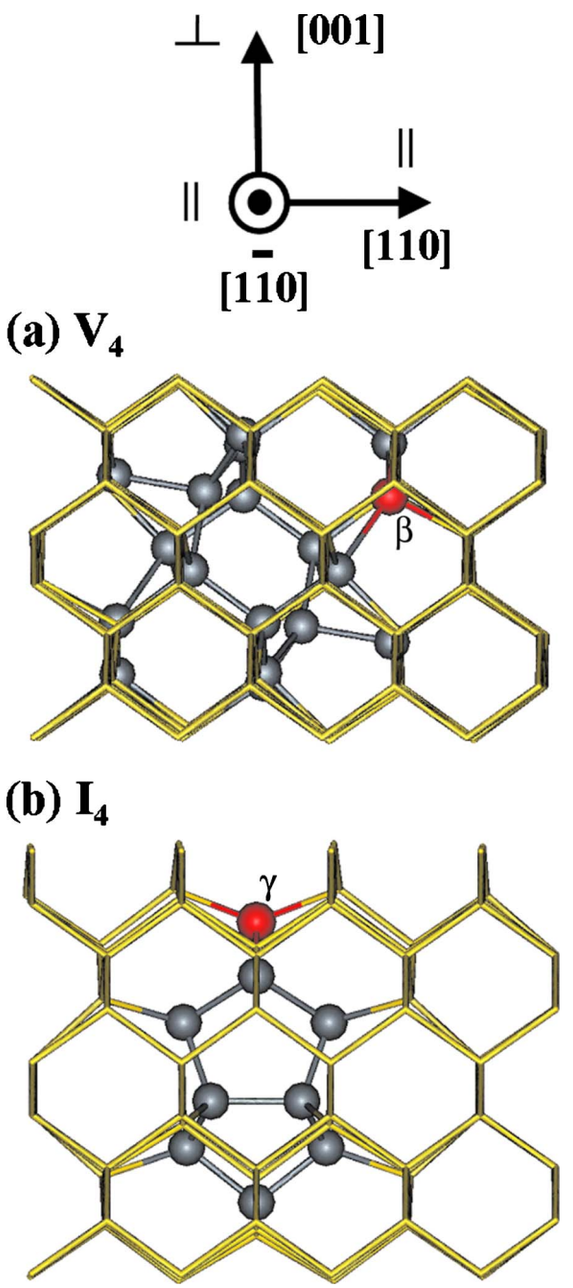

Figure 1. (Color online) Strain-free representations of V_4 (a) and I_4 (b) clusters shown embedded inside subsections of their respective 480-atom supercells. Light gray (gold) wireframe represents bulk Si atoms in the lattice. Dark gray spheres represent interstitial atoms comprising the cluster (I_4 only) as well as highly-strained atoms adjacent to the cluster cores (V_4 and I_4). The atoms representing the highest strain energy in each case (V_4, atom β; I_4, atom γ) are labeled and colored (red). The out-of-plane and in-plane directions for biaxial strain are depicted with the crystallographic axes.

lationship between out-of-plane and in-plane strain using tabulated elastic stiffness constants (C_{ij}):[29] $\nu^* = -\varepsilon_\perp/\varepsilon_\parallel = 2(C_{12}/C_{11}) = 0.771$. The upper panel of Fig. 1 shows the biaxial strain scheme with crystallographic reference. Using $\nu^* = 0.771$, $\varepsilon_\parallel = (a_\parallel - a_{Si})/a_{Si}$, and $\varepsilon_\perp = (a_\perp - a_{Si})/a_{Si}$, we calculated values of out-of-plane $a_{Si}(a_\perp)$ for each independent value of in-plane a_{Si} $(a_\parallel)$ to appropriately scale additional supercell dimensions representing ±3% biaxial strain. We numerically verified that minimum energy supercell dimensions occur as ν^* converges to the theoretical value of 0.771.

Conditions of ±3% strain (tensile is positive) were chosen to best illustrate our results (±1, ±2, and ±4% strain were also studied). We investigated Si biaxial strain within the range of ±4% strain because 4% tensile strain is the limiting case of epitaxial Si grown on pure Ge.[30] Compressive biaxial films could be realized on alloy substrates ($Si_{1-x}C_x$) of the diamond structure. Therefore, while ±3% strain conditions are large in high-density microelectronic integration (typical magnitudes are $|\varepsilon| < 1\%$),[31] these magnitudes are feasible in the laboratory. There is currently little precedence for strained *c*-Si in solar cells; however, strain engineering could be applied to photovoltaics. As in microelectronic fabrication, strategic material selection, such as the metal backplane in a conventional solar cell, or engineered process conditions, such as annealing treatments, could be used to implement strain in thin film *c*-Si absorption layers.

Improved descriptions[32-34] of the aggregation and behavior of Si point defects following ion implantation were fueled by the development of microelectronic fabrication process simulators. Previous theoretical works by Makhov and Lewis[35] (V_4) and Arai et al.[36] (I_4) proposed the importance of FC configurations for specific cluster sizes (n). The recent endeavors of Lee and co-workers[37,38] generalize the significance of FC Si native defect clusters by detailing their thermodynamic favorability through application of an integrated atomistic modeling procedure for small n (V_n, $n \leqslant 48$; I_n, $n \leqslant 16$). Our recent work[30,39] describes the influence of uniform strain fields on the stability, structure, and orientation of these same clusters. We use the V_4 and I_4 clusters in this article to represent general FC cluster behavior. Based on our previous work,[30,38] only neutral-state clusters were considered because FC configurations are unlikely to ionize under intrinsic conditions. The embedded configurations of V_4 and I_4 are illustrated in Fig. 1a and b, respectively. For each structure, the atom representing the highest strain energy (degeneracy creates additional candidates), as calculated using a Keating-type parameterization of the Si network,[30] is annotated for discussion.

Figure 2 shows the $\alpha(\omega)$ spectra for *c*-Si, V_4, and I_4 subjected to various biaxial strain conditions. Note that the absorption edge in the $\alpha(\omega)$ plots is modified from the fundamental E_g in two ways: (1) the indirect nature of Si precludes significant optical transitions from occurring at the 1.11 eV bandgap, so the main transitions begin at higher energies where the first direct transitions are possible,[1] and (2) DFT E_g underestimation tends to reduce calculated direct transition energies. In Fig. 2a, it is apparent that biaxial strain of either sign redshifts the onset of absorption (E_0 transition),[1] where the greater absorption enhancement is seen for the tensile case. We observed similar behavior at other strain magnitudes (±1, ±2, and ±4%) and verified that the magnitude of redshift (enhancement) in absorption onset correlates with the applied strain magnitude. In Fig. 2b and c, the inception of low-energy optical absorption is redshifted by nearly 2 eV in the presence of either FC cluster embedded in strain-free Si. In Fig. 2b, incipient absorption for strain-free V_4 occurs at 0.48 eV, which reduces to 0.23 (0.17) eV under 3% tensile (compressive) biaxial strain. Similarly, in Fig. 2c, incipient absorption for strain-free I_4 occurs at 0.55 eV, which reduces to 0.37 (0.10) eV under 3% compressive (tensile) biaxial strain. Note that the observed optical response is complementary with respect to the structural strain configuration: V_4 imparts a tensile local strain field on the lattice and is consequently stabilized by applied compression; likewise, I_4 imparts a compressive local strain field on the lattice and is consequently stabilized by applied tension. These results suggest that characteristic optical absorption in *c*-Si can be modified through manipulation of the comprehensive strain field profile.

To better understand the complementary behavior exhibited in optical absorption, we examined the LDOS of atoms selected through inspection of atomistic strain profiles. Searching for a po-

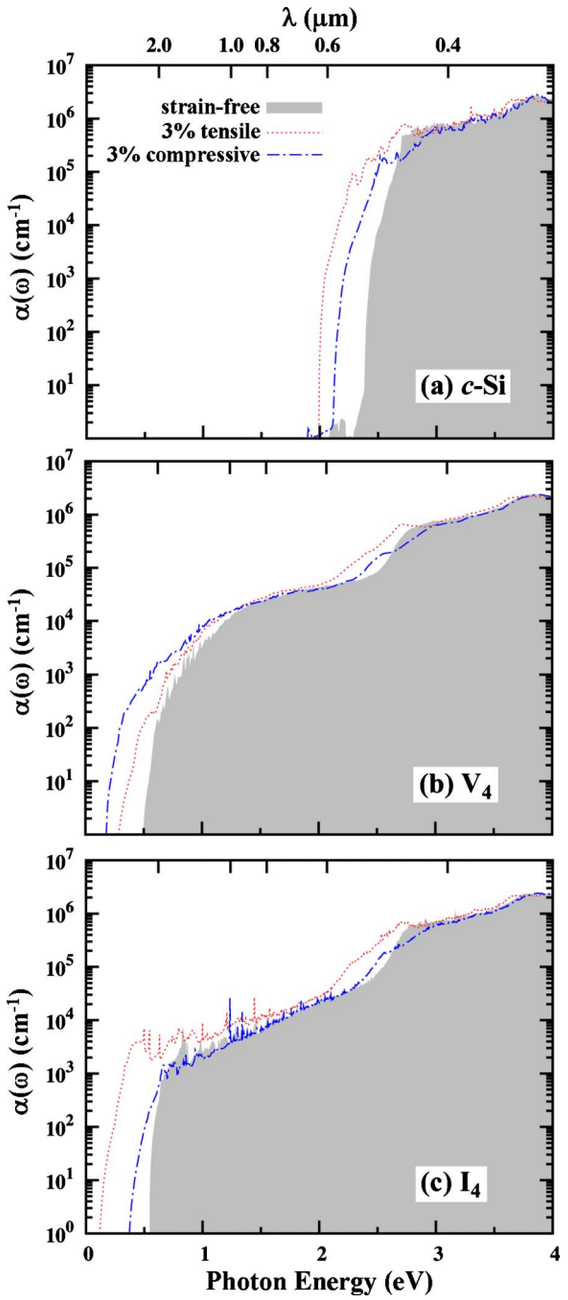

Figure 2. (Color online) Absorption coefficient spectra from DFT-GGA calculations for (a) *c*-Si, (b) V_4, and (c) I_4 structures using 480-atom supercells under various biaxial strain conditions. In each plot, the gray-filled region represents the reference $\alpha(\omega)$ for the strain-free structure.

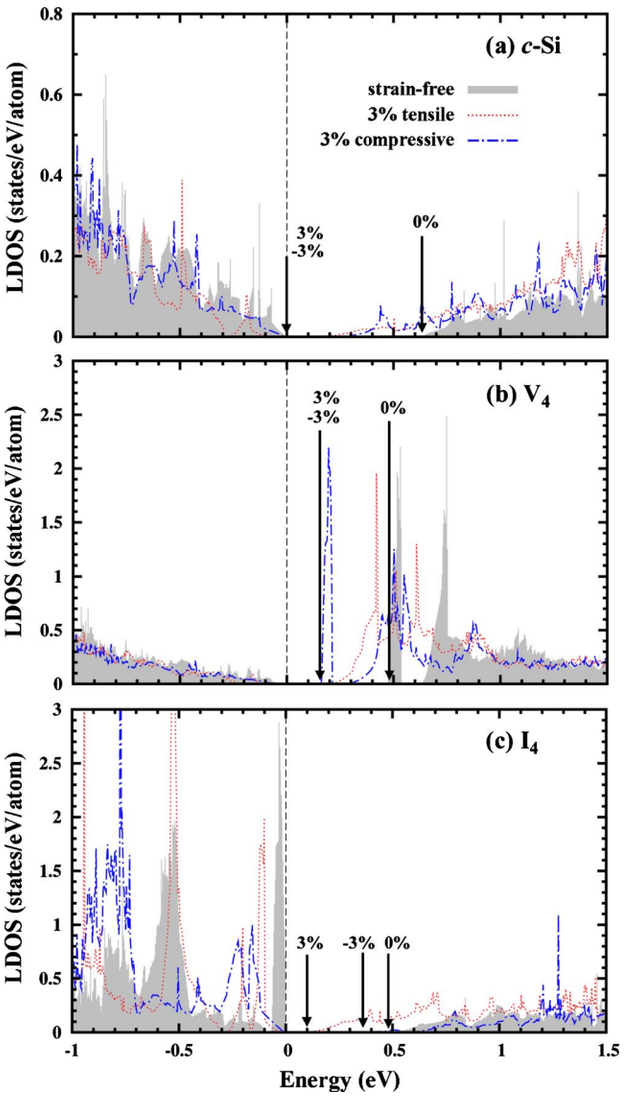

Figure 3. (Color online) Local density of states near the Si bandgap for (a) *c*-Si, (b) V_4, and (c) I_4 projected onto respective atoms representing the highest strain energy for the clusters (V_4, atom β; I_4, atom γ) and an arbitrary atom for *c*-Si. In each plot, the gray-filled background spectra represents the reference LDOS under strain-free conditions. All LDOS spectra are referenced to their respective valence band maxima as indicated by dashed black reference lines and respective Fermi energies for each strain condition are indicated by vertical, black arrows.

tential structural connection to the observed absorption phenomena, we reviewed the LDOS character at the compressive and tensile extrema (atomic sites) for both clusters; however, a complementary LDOS relationship between dominant valence band (VB) and conduction band (CB) character was not readily apparent within the same structure. Instead, we proceeded to analyze the effect of variable applied strain conditions on the atomic site representing the highest strain energy in each structure. These results are collectively presented in Fig. 3 for each case. The complementary LDOS behavior originally anticipated is present when the V_4 LDOS at atom β is compared to the I_4 LDOS at atom γ. Consistent with the results of Pan et al.,[12] increased CB character is observed with the longer bonds associated with the locally-tensile strain field around V_4, while increased VB character is observed with the shorter bonds associated with the locally-compressive strain field around I_4.

Furthermore, evaluation of the LDOS dependence on applied strain reveals that the primary reason for increased optical absorption in each case is an effectively shrinking E_g that correlates with observed redshifting in $\alpha(\omega)$. For V_4, we also observe a prominent distribution of IB states, which can be manipulated by strain, that can reduce the minimum energy required to absorb an incident photon and lower the effective E_g similar to studies of IB solar cell materials that rely on transition metal doping.[4,5] In both V_4 cases ($\varepsilon = -3$ and 0%) containing the IB peak, the Fermi level is also located at the IB peak, which suggests partial band occupation that satisfies one requirement for multistage photon absorption.[4] With this multigap perspective, the smallest E_g gating V_4 absorption among the three strain cases is observed under compressive strain

between the VB and prominent IB peak, while the smallest E_g in both the *c*-Si and I_4 cases occurs under tensile conditions.

In summary, our DFT calculations predict optical absorption enhancement (redshift) in *c*-Si in the presence of either vacancy (V_4) or interstitial (I_4) FC clusters that can be further enhanced by biaxial strain. Although applied strain improves absorption in all cases studied ($\varepsilon = -3$, 0, and 3%), compressive strain exhibits the largest enhancement on V_4, while tensile strain exhibits the largest enhancement on I_4. LDOS examination of the most-strained atom in each structure reveals that the primary reason for increased absorption correlates with a decreased bandgap, including an IB for V_4 under certain strain conditions.

Acknowledgments

We acknowledge the National Science Foundation (CAREER-CTS-0449373) and the Robert A. Welch Foundation (F-1535) for their financial support. S. L. is grateful for support from the Donald D. Harrington Graduate Fellows Program. We would also like to thank the Texas Advanced Computing Center for use of their computing resources.

The University of Texas at Austin assisted in meeting the publication costs of this article.

References

1. P. Y. Yu and M. Cardona, *Fundamentals of Semiconductors*, Springer-Verlag, New York (2001).
2. C. R. Wronski, B. von Roedern, and A. Kolodziej, *Vacuum*, **82**, 1145 (2008).
3. D. E. Carlson and C. R. Wronski, *Appl. Phys. Lett.*, **28**, 671 (1976).
4. P. Palacios, I. Aquilera, K. Sánchez, J. C. Conesa, and P. Wahnón, *Phys. Rev. Lett.*, **101**, 046403 (2008).
5. K. Sánchez, I. Aguilera, P. Palacios, and P. Wahnón, *Phys. Rev. B*, **79**, 165203 (2009).
6. T. Stelzner, M. Pietsch, G. Andrä, F. Falk, E. Ose, and S. Christiansen, *Nanotechnology*, **19**, 295203 (2008).
7. S. Knief and W. von Niessen, *Phys. Rev. B*, **59**, 12940 (1999).
8. H. J. Stein, F. L. Vook, and J. A. Borders, *Appl. Phys. Lett.*, **14**, 328 (1969).
9. P. J. Foster, J. K. Doylend, P. Mascher, A. P. Knights, and P. G. Coleman, *Proc. SPIE*, **5577**, 683 (2004).
10. H. A. Weakliem and D. Redfield, *J. Appl. Phys.*, **50**, 1491 (1979).
11. B. G. Streetman, *Solid State Electronic Devices*, Prentice Hall, Upper Saddle River, NJ (1995).
12. Y. Pan, F. Inam, M. Zhang, and D. A. Drabold, *Phys. Rev. Lett.*, **100**, 206403 (2008).
13. J. P. Perdew and Y. Wang, *Phys. Rev. B*, **45**, 13244 (1992).
14. G. Kresse and J. Hafner, *Phys. Rev. B*, **47**, 558 (1993); G. Kresse and J. Hafner, *Phys. Rev. B*, **49**, 14251 (1994); G. Kresse and J. Furthmüller, *Comput. Mater. Sci.*, **6**, 15 (1996); G. Kresse and J. Furthmüller, *Phys. Rev. B*, **54**, 11169 (1996).
15. G. Kresse and J. Furthmüller, *VASP the Guide*, Vienna University of Technology, Vienna (2001).
16. P. E. Blöchl, *Phys. Rev. B*, **50**, 17953 (1994).
17. J. Furthmüller, http://www.freeware.vasp.de/VASP/optics, last accessed November 2, 2010.
18. R. J. Bondi, S. Lee, and G. S. Hwang, *Phys. Rev. B*, **81**, 195207 (2010).
19. R. J. Bondi, S. Lee, and G. S. Hwang, *Phys. Rev. B*, **82**, 115214 (2010).
20. M. Marsman, J. Paier, A. Stroppa, and G. Kresse, *J. Phys.: Condens. Matter*, **20**, 064201 (2008).
21. J. Furthmüller, G. Cappellini, H.-Ch. Weissker, and F. Bechstedt, *Phys. Rev. B*, **66**, 045110 (2002).
22. S. Zh. Karazhanov, P. Kroll, A. Holt, A. Bentzen, and A. Ulyashin, *J. Appl. Phys.*, **106**, 053717 (2009).
23. P. Kempisty, S. Krukowski, P. Strak, and K. Sakowski, *J. Appl. Phys.*, **106**, 054901 (2009).
24. N. Umezawa, K. Shiraishi, T. Ohno, H. Watanabe, T. Chikyow, K. Torii, K. Yamabe, K. Yamada, H. Kitajima, and T. Arikado, *Appl. Phys. Lett.*, **86**, 143507 (2005).
25. B. Xu, J. Yin, Y. D. Xia, X. G. Wan, K. Jiang, and Z. G. Liu, *Appl. Phys. Lett.*, **96**, 163102 (2010).
26. F. Gao, J. Qu, and M. Yao, *Appl. Phys. Lett.*, **96**, 102108 (2010).
27. P. Bhattacharya, *Semiconductor Optoelectronic Devices*, Prentice Hall, Upper Saddle River, NJ (1997).
28. J. Singh, *Physics of Semiconductors and Their Heterostructures*, McGraw-Hill, New York (1993).
29. M. E. Levinshtein, S. L. Rumyantsev, and M. S. Shur, *Handbook Series on Semiconductor Parameters*, Vol. 1, p. 29, World Scientific, London (1996).
30. R. J. Bondi, S. Lee, and G. S. Hwang, *Phys. Rev. B*, **79**, 104106 (2009); R. J. Bondi, S. Lee, and G. S. Hwang, *Phys. Rev. B*, **80**, 125202 (2009); R. J. Bondi, S. Lee, and G. S. Hwang, *Appl. Phys. Lett.*, **94**, 264101 (2009).
31. K.-J. Chui, K.-W. Ang, N. Balasubramanian, M.-F. Li, G. S. Samudra, and Y.-C. Yeo, *IEEE Trans. Electron Devices*, **54**, 249 (2007).
32. S. S. Kapur, M. Prasad, J. C. Crocker, and T. Sinno, *Phys. Rev. B*, **72**, 014119 (2005).
33. M. Y. L. Jung, R. Gunawan, R. D. Braatz, and E. G. Seebauer, *J. Electrochem. Soc.*, **151**, G1 (2004).
34. S. Chakravarthi and S. T. Dunham, *J. Appl. Phys.*, **89**, 4758 (2001).
35. D. V. Makhov and L. J. Lewis, *Phys. Rev. Lett.*, **92**, 255504 (2004).
36. N. Arai, S. Takeda, and M. Kohyama, *Phys. Rev. Lett.*, **78**, 4265 (1997).
37. S. Lee and G. S. Hwang, *Phys. Rev. B*, **77**, 085210 (2008); S. Lee and G. S. Hwang, *Phys. Rev. B*, **78**, 045204 (2008); S. Lee and G. S. Hwang, *Phys. Rev. B*, **78**, 125310 (2008).
38. S. Lee, R. J. Bondi, and G. S. Hwang, *Phys. Rev. B*, **80**, 245209 (2009).
39. R. J. Bondi, S. Lee, and G. S. Hwang, *Phys. Rev. B*, **81**, 245206 (2010).